Materials and Design 61 (2014) 177–184

Contents lists available at ScienceDirect

Materials and Design

journal homepage: www.elsevier.com/locate/matdes

Finite element analysis of bone loss around failing implants

Jan Wolff [a,g], Nathaniel Narra [b,e,*], Anna-Kaisa Antalainen [c], Jiří Valášek [d], Jozef Kaiser [h], George K. Sándor [i,f], Petr Marcián [d]

[a] Department of Oral and Maxillofacial Surgery/Oral Pathology, VU University Medical Center, Amsterdam, The Netherlands
[b] Department of Electronics and Communications Engineering, Tampere University of Technology, Finland
[c] Department of Oral Radiology, Institute of Dentistry, University of Helsinki, Helsinki, Finland
[d] Institute of Solid Mechanics, Mechatronics and Biomechanics, Faculty of Mechanical Engineering, Brno University of Technology, Czech Republic
[e] BioMediTech, Institute of Biosciences and Medical Technology, Tampere, Finland
[f] Department of Oral and Maxillofacial Surgery, Oulu University Hospital, University of Oulu, Oulu, Finland
[g] Oral and Maxillofacial Unit, Department of Otorhinolaryngology, Tampere University Hospital, Tampere, Finland
[h] X-ray, MicroCT and NanoCT Research Group, CEITEC - BUT, Brno University of Technology, Czech Republic
[i] Institute of Biomedical Technology, University of Tampere, Finland

ARTICLE INFO

Article history:
Received 10 February 2014
Accepted 29 April 2014
Available online 9 May 2014

Keywords:
Dental implant
Peri-implantitis
Finite element analysis
Bone loss
Implant geometry

ABSTRACT

Dental implants induce diverse forces on their surrounding bone. However, when excessive unphysiological forces are applied, resorption of the neighbouring bone may occur. The aim of this study was to assess possible causes of bone loss around failing dental implants using finite element analysis. A further aim was to assess the implications of progressive bone loss on the strains induced by dental implants. Between 2003 and 2009 a total of 3700 implant operations were performed in a private clinic. Ten patients with 16 fixtures developed severe marginal bone defects. Finite element analysis was used to assess the effective strains produced at the bone-implant interface under unidirectional axial loading. These simulations were carried out on 4 specific implant types – Camlog Plus, Astra Osseo Speed, Straumann BL and Straumann S/SP. All implant types exhibited degraded performance under circular and horizontal bone loss conditions. This is evidenced by increased distribution of pathological strain intensities (>3000 με), in accordance with the mechanostat hypothesis, in the surrounding bone. Among the implants, the Camlog design seemed to have performed poorly, especially at the chamfer in the implant collar (>25000 με). Implants are designed to perform under nearly ideal conditions from insertion till osseointegration. However, when the surrounding bone undergoes remodelling, implant geometries can have varied performance, which in some cases can exacerbate bone loss. The results of this study indicate the importance of evaluating implant geometries under clinically observed conditions of progressive bone loss.

1. Introduction

When dental implants are placed into bone it is expected that they will remain functional for a lifetime; however complications do occur. According to Esposito et al., implant failures can be categorised chronologically into 'early failures' and 'late failures' [1]. It is suggested that early failures occur before abutment connection and occlusal loading. Such failures are often caused by interferences in the initial healing process leading to non-integration of the implant. Late failures have been described as occurring after occlusal loading [2]. According to Koldsland et al., most failures tend to occur at an early stage, that is, before occlusal loading [3]. One common cause of interference in the initial healing process is surgical trauma. The drilling forces induced intraoperatively are very subjective and are influenced by the perceptual and motor skills of the clinician involved. When excess forces are applied during drilling, mechanical and thermal damage can occur to the surrounding bony tissue and thereby jeopardize the establishment of osseointegration [4].

Adaptive changes that take place when bone loading occurs can influence the initial healing process, a phenomena first described by Wolff in 1892 [5]. In the 1960s, Frost introduced the mechanostat hypothesis that is a refinement of Wolff's law [6]. The hypothesis attributes strain values between 1000 με and 1500 με to be physiological, which can be attained during normal mastication.

* Corresponding author at: Department of Electronics and Communications Engineering, Tampere University of Technology, Finn-Medi 1 L 4, Biokatu 6, Tampere 33520, Finland. Tel.: +358 40 8490166; fax: +358 3 3641385.
E-mail address: nathaniel.narragirish@tut.fi (N. Narra).

http://dx.doi.org/10.1016/j.matdes.2014.04.080
0261-3069/

Table 1
Details of failed/failing implants observed in the clinical case pool.

Case no.	Sex	Age	Time (months)	Loss type	Region	Implant type	Dimensions (mm)
1	F	33	2	Circular	46	Camlog Plus	5 × 11
2	M	64	1	Circular	36	Camlog Plus	5 × 11
3	F	42	3	Circular	36	Camlog Plus	3.8 × 9
4	F	46	2	Circular	36	Camlog Plus	3.8 × 11
					37	Camlog Plus	3.8 × 9
5	F	60	1	Circular	47	Camlog Plus	4.3 × 11
6	M	53	9	Horizontal	13	Camlog Plus	4.3 × 11
					14		4.3 × 11
					15		4.3 × 9
					22		3.8 × 11
					24		3.8 × 11
					26		4.3 × 9
7	F	68	5	Circular	14	Straumann BL	4.1 × 10
8	F	55	3	Circular	47	Astra Osseo Speed	4 × 11
9	F	83	12	Circular	47	Straumann S	4.1 × 12
10	F	56	4	Circular	36	Straumann SP	4.1 × 10

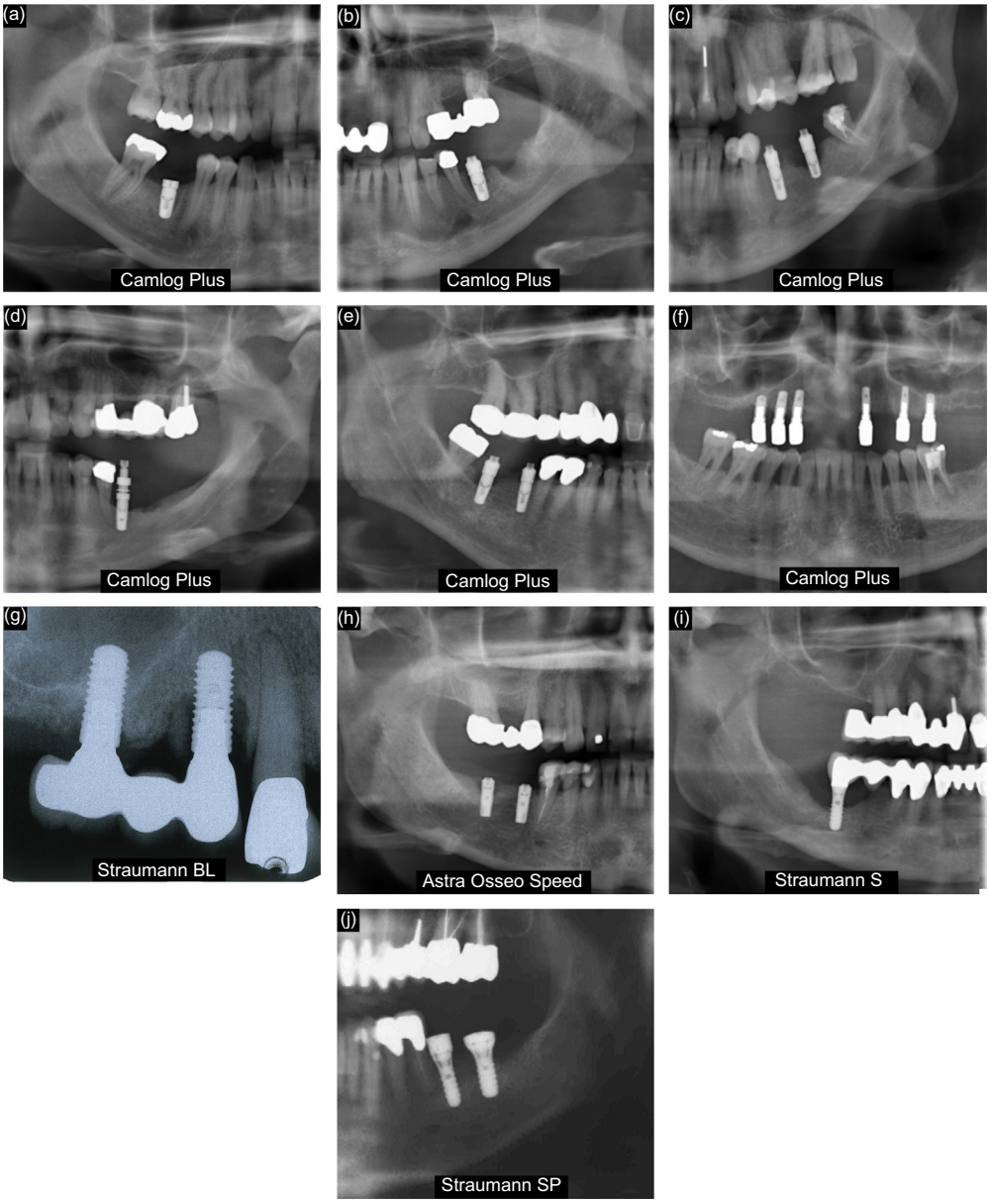

Fig. 1. Radiographs demonstrating circular and horizontal bony defects observed around implants.

However when strain values greater than 1500 με are induced, a hypertrophic increase in modelling and an associated decrease in remodelling can occur. When peak strains exceed values of 3000 με the structural integrity of the bone is endangered and can, in some cases, result in pathologic overload.

These high pathological strains can be induced in the surrounding bone during implant placement when high torque values (>45 N cm) are applied. Over tightening which leads to bone compression, often results in necrosis of the bone and in some cases can result in implant failure [7]. Such compressive forces are dictated by the implant geometry. Until recently the majority of dental implants have had a cylindrical shape, though currently the trend is towards developing tapered implants that resemble tooth roots, which are supposed to have better stress transfer into surrounding bone [8].

In order to evaluate the effect of implant geometry on the strain distribution patterns, it is essential to use computational models. Finite element analysis (FEA) is an ideal method for modelling complex structures and analysing their mechanical behaviour [9–12]. Advances in imaging technology have made it possible to image bone and implant structures at the microlevel in 3D. This makes it possible to construct very accurate anatomical models which in turn give reliable results.

Considering the large variation in implant geometries on the market, better understanding of the effect of geometry on the surrounding bone tissue is of great clinical relevance. The aim of this study was to assess the effect of 4 different implant geometries on the strain distributions in the loaded bone leading to bone loss using FEA. Furthermore, based on clinical cases, the consequences of bone loss around failing implants, and the corresponding changes in the strain distribution patterns were assessed. As of date, very little research has been done investigate the effect of progressive bone loss on the strain distribution around dental implants. Thus the progressive performance of these implants consequent to clinically observed bone loss is of particular interest.

2. Materials and methods

2.1. Patient information

Between the years 2003 and 2009, 3700 maxillary and mandibular reconstructions, employing dental implants to rehabilitate

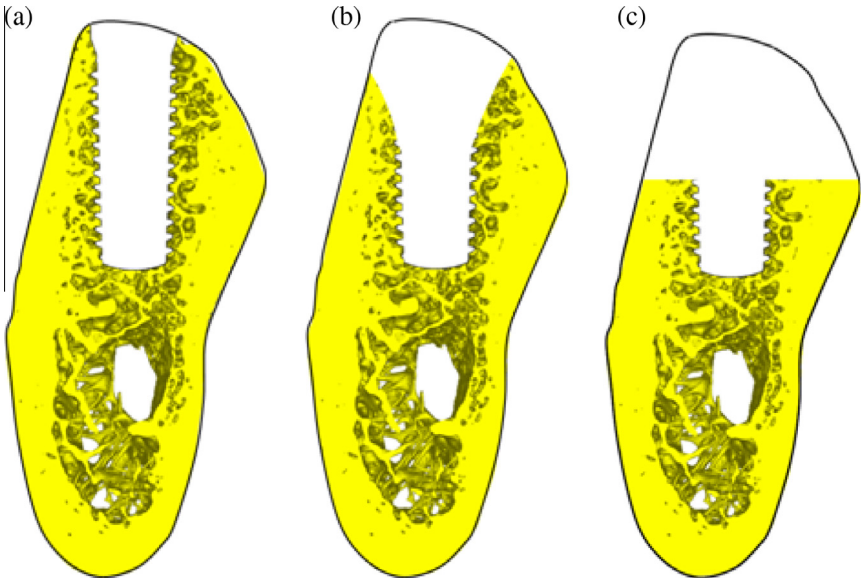

Fig. 2. Scheme of surrounding bone model used in the simulations – (a) full bone, (b) circular bone loss, (c) horizontal bone loss.

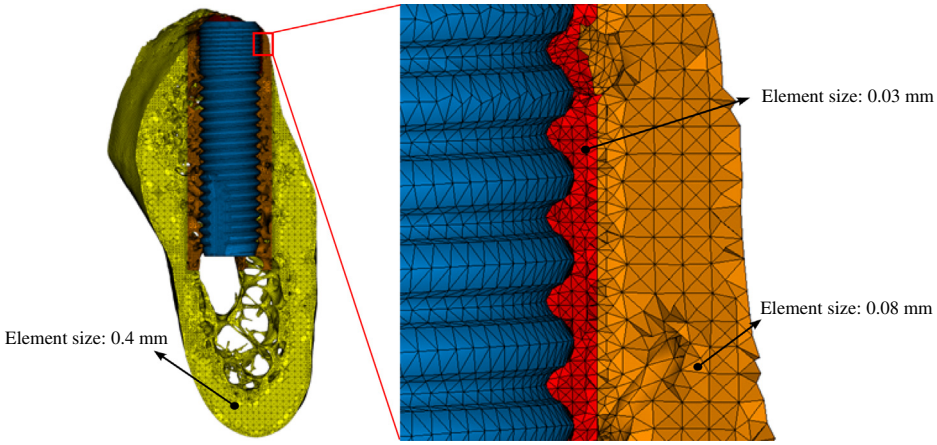

Fig. 3. The different element sizes contained in the mesh representing bone tissue. At the bone-implant interface, bone is specifically refined for consistence with the adjacent implant threads. Thus, micro-threads present in the Astra implant (as illustrated) justify an element size of 0.03 mm.

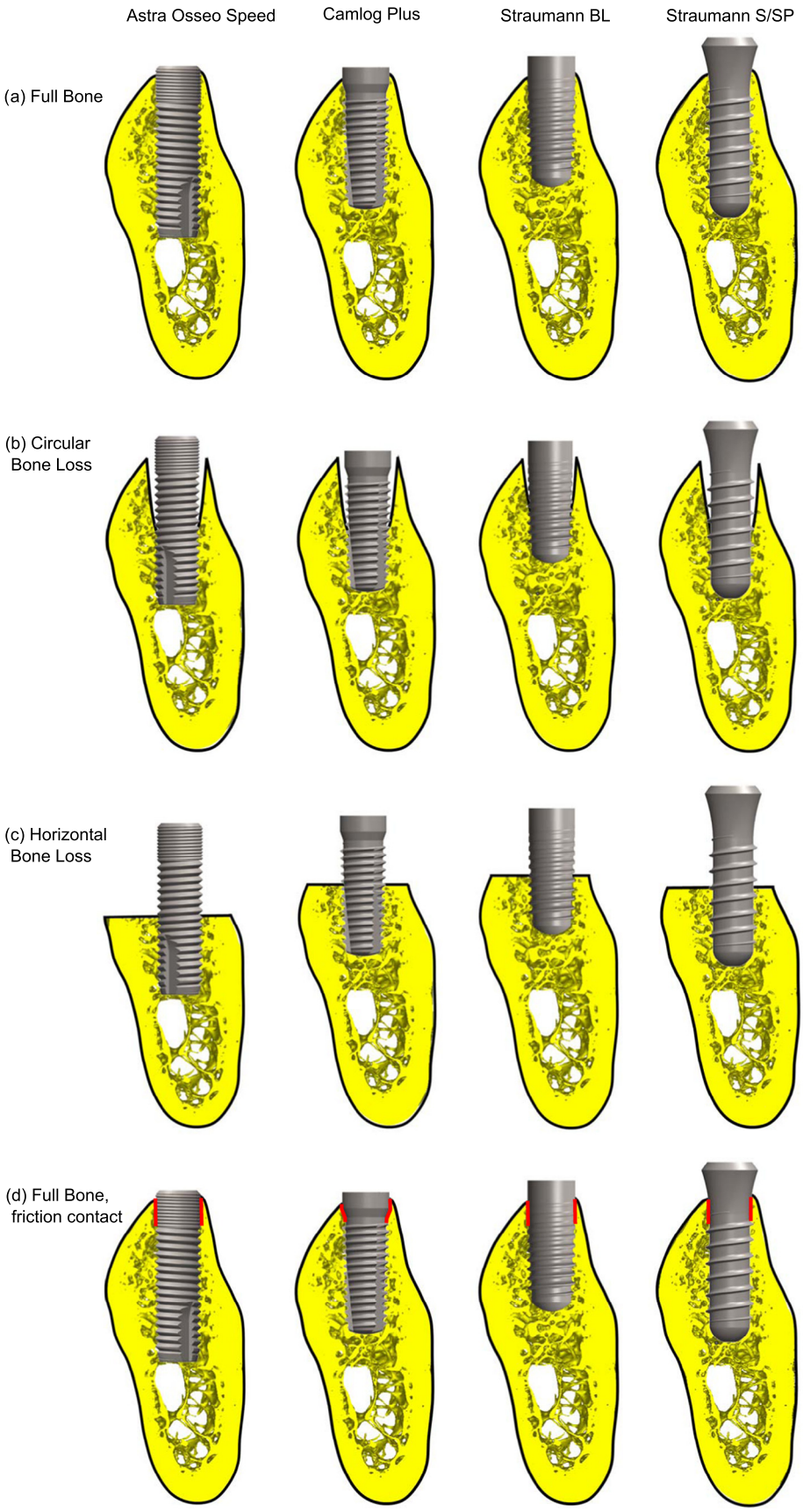

Fig. 4. Schematic representation of the 16 bone and implant configurations simulated for induced strains. The red marker (last row) indicates the extent of the region where frictional contact is defined at the bone-implant interface. For a colour representation, the reader is referred to the online version of this paper. (For interpretation of the references to colour in this figure legend, the reader is referred to the web version of this article.)

masticatory function, were performed at a private clinic for oral surgery in Hamburg Germany by one oral surgeon. All patients were randomly allocated by the referring dentists to three different implant systems (Straumann AG, Basel, Switzerland; Camlog, Biotechnologies AG, Basel, Switzerland and Astra Tech AB, Gothenburg, Sweden). Informed consent was obtained from all patients included in this study. Before implant treatment, all patients were screened for pre-existing dental problems and systemic health. All patients were treated using a standardized two-stage surgical implant placement procedure. Antibiotic coverage with amoxicillin (250 mg) had been given 1 h before surgery and every 6 h after surgery for three days. For patients allergic to penicillin, erythromycin (250 mg) was used. Chlorhexidine (0.12%) mouth rinse was also used topically for 2 weeks after surgery.

In the six year observation period, 10 patients (8 females and 2 males, average age 56 years) were diagnosed with peri-implantitis having developed circular and horizontal bony defects requiring surgical treatment (Table 1). These defects were observed in the follow-up radiographs shown in Fig. 1. The radiographs in this study were used with patient consent.

2.2. Peri-implantitis treatment protocol

Following the administration of local anaesthesia, a full-thickness flap was elevated and the granulation tissue was then removed. The largely exposed titanium implant surface was then subsequently cleaned with gauze soaked in 1% chlorhexidine gel. The peri-implant bone defects were then filled with a mixture of autogenous bone chips and de-proteinized bovine bone mineral granules (size: 1.0–2.0 mm; Bio-Oss®, Geistlich Pharma AG, Switzerland). The soft tissues were repositioned by tension-free suturing. A systemic administration of antibiotics was combined with the surgical protocol. Postoperative follow-up included clinical examination and radiographs. The follow-up period ranged from 1 to 3 years after surgical debridement and augmentation with bovine bone mineral granules.

2.3. Finite element analysis

Simulations were performed on 4 implant types (Camlog Plus, Astra Osseo Speed, Straumann BL and Straumann S/SP) to assess the effect of their geometries on the distribution of strain in the surrounding bone tissue. To obtain the geometrical model of the surrounding bone a cadaveric mandibular bone segment was imaged in a micro-CT device ($1984 \times 1984 \times 2175$ image volume with 17 μm isometric voxels). The image data was used to generate a Standard Tessellation Language (STL) model of the bone segment using STL Model Creator [13] programmed in MATLAB 2012 (MathWorks, Natick, MA, USA). Subsequently the geometrical model of the bone was edited in Magics (Materialise, Lueven, Belgium) to create three configurations. These configurations correspond to normal bone structure and two types of bone loss patterns observed in the clinical cases (Fig. 1). For implant geometry, four implants identical to those used in the study patients (Fig. 2) were scanned with a high resolution ATOS optical 3D scanner (GOM mbH, Braunschweig, Germany). The point cloud information was used to generate computer models using SolidWorks 2012 (Dassault Systems, Vélizy-Villacoublay, France). It should be noted that while Straumann S and SP implants are different products, they both have the exact same geometry in the region that is inserted into the bone. They only differ in the length of the implant collar which does not affect the simulations performed in this study; where forces are applied uni-directionally along the long axis of the implant. The acquired bone and implant models were assembled into a three-dimensional finite element mesh structure. The individual components were meshed and assembled in ANSYS 14 (Swanson Analysis Systems Inc., Houston, PA, USA). The implants were inserted into the model of bone in the exact same location. All model volumes were discretized by 10-node quadratic tetrahedral elements with three degrees of freedom (SOLID187). Bone tissue was modelled at three different levels of discretization (Fig. 3). The bone-implant interface was modelled with finer element sizes to enhance accuracy of results in the tissue in close proximity to the implant threads (Fig. 3). The mesh representing bone adjacent to the micro-threads in Astra implant was further refined to an element size of 0.03 mm. Contact elements CONTA175 and TARGE170 were used to model the bone-implant interface. The total number of elements in the models range from 6 to 7.5 million with approximately 7–10 million nodes. The finite element mesh was checked to avoid error elements.

The material properties of bone tissue and the dental implants were defined using a homogeneous isotropic linearly elastic material model, explicitly described by two parameters: Young's modulus (E) and Poisson's ratio (μ). For titanium implant these were defined as $E = 110{,}000$ MPa and $\mu = 0.3$ [14–16]. The trabecular and cortical bone material characteristics were assumed to be similar at the micro-level in keeping with literature [17,18]. Thus, similar material properties were used for both bone tissues; specifically $E = 13\ 700$ MPa and $\mu = 0.3$ [19–23].

A total of four different configurations were constructed for each of the four implant geometries (Camlog, Astra, Straumann BL and Straumann S/SP). The configurations included two pathological conditions observed in the patients – circular bone loss and horizontal bone loss. In addition, the full bone model (without pathological resorption) was simulated under two conditions which differed in the extent and type of bone-implant contact (BIC). A clinically osseointegrated implant is where the surrounding bone morphology is healthy and the implant surface and adjacent bone tissue fuse to form a sturdy interface. In the FEA procedure this condition is simulated by defining the bone-implant interface of the model mesh as 'bonded always'. In this study this configuration is referred to as – full bone bonded. Another configuration was created to simulate the situation where the BIC in the region of the implant neck degrades, specifically within the cortical bone. This can occur due to various reasons, such as over-torqueing during insertion resulting in non-fusion of bone and implant, or pathology in bone tissue when implant geometry induces localised high strains. This condition is simulated by defining the bone-implant interface as a 'friction' contact. In this study this configuration is referred to as – full bone friction. A friction contact allows for minor tangential displacements between the implant and bone at the interface. In this study the friction coefficient was set to 0.3 [15]. In all configurations the implants were axially loaded with 200 N on the uppermost cross section of the implant based on literature [24]. All nodes at the mesial and distal borders of the mandibular bone segment were fixed in all directions to

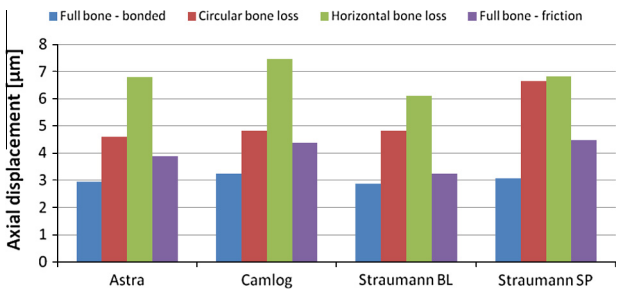

Fig. 5. Observed axial displacements (μm) in the four implants in four different configurations, under uni-axial loads of 200 N.

represent continuity within the mandible. Small displacements were considered during solution, as simulations with large displacement did not converge. Effective strain was selected as a value for analysis of bone tissue [12,25–28].

3. Results and discussion

A total of 4 bone model configurations (full bone bonded, circular bone loss, horizontal bone loss and full bone friction) were simulated for each of the 4 implant types (Astra, Camlog and two Straumann; Fig. 4). The axial displacements ranged from 2.9 to 7.5 μm (Fig. 5). Among the bone configurations, the largest displacements were observed in the horizontal bone loss models, with the highest in the Camlog implant (7.5 μm). The full bone bonded configuration displayed the least differences between the implants. In full bone friction configuration, the Straumann BL implant displayed the least displacement (3.3 μm). The difference in implant displacement magnitudes between the full bone bonded and full bone friction configurations (for a given implant) was insignificant (maximum difference ~1 μm).

Fig. 6. Differences in strain intensity (με) distribution in the adjacent bone at the bone-implant interface for – (a) full bone bonded, (b) circular bone loss, (c) horizontal bone loss and (d) full bone friction; in the four implants. Schemes in the leftmost column illustrate the bone morphology used in simulating corresponding configurations. The red marker in (d) indicates the region where frictional contact is defined instead of 'bonded always'. For a colour representation, the reader is referred to the online version of this paper. (For interpretation of the references to colour in this figure legend, the reader is referred to the web version of this article.)

The effect of applied loads on the bone-implant interface was observed in terms of strains induced in the bone tissue [29–31]. All strains are displayed in the corono-apical cut of the simulation results. The colour ranges were changed to correspond to strain intensity intervals (in micro-strain, με) suggested by mechanostat hypothesis (Fig. 6). In Fig. 6, each subfigure represents the results of simulation of a configuration in the corresponding location in Fig. 4.

In the full bone bonded configuration, in all implants, the strains induced in the bone next to the threads are largely less than 1500 με (Fig. 6a). However in the implant neck region the Camlog implant showed an increased prevalence of high strains in comparison to the other two implants. Nonetheless, the unphysiological strain regions (in red) are minimal in area. In the bone loss model configurations (circular and horizontal, Fig. 6b and c) the strain magnitudes increase significantly, with greater regions of unphysiological strains (>3000 με) in all 4 implants types. In the full bone friction configuration (Fig. 6d), Astra implant induces minimal regions of unphysiological strain. The Straumann and Camlog implants induce considerable regions of high strains in the bone, with the bone adjacent to the neck of the Camlog implant particularly overloaded. The bone adjacent to the chamfer in the Camlog implant is subjected to more than 25,000 με (Fig. 7), which is beyond the fracture limit of bone [6].

The results offer an insight into the performance of geometrically different implants under conditions of bone loss. Once bone degradation in the cortical bone commences, the differences in geometry between the implants becomes apparent. Of the four, the Astra and Straumann geometries seem to offer better distribution of strains, even with adjacent bone loss. Of particular note, when the model was simulated with full osseointegration with no bone loss, the Astra implant seems to perform similarly to the Straumann implant. A possible reason for this is that the Astra and Straumann implants by their design have their threads in the cortical bone, whereas in Camlog a smooth surface interfaces with the cortical bone. Thus, the results indicate that the presence of implant micro-threads in the cortical bone may have a positive influence on the strain distribution.

In the clinical experience of the authors the Camlog implants exhibited a high incidence of complications resulting from rapid bone loss. Thus more detailed simulations were performed under conditions simulating relative bone movement at the implant surface in the upper part of the implant. Under these conditions (friction contact) the simulations revealed that the chamfer at the neck induces very high strains in a very small region (Fig. 7). In clinical practice this particular implant site is surrounded by cortical bone. Thus a possible explanation for the observed clinical outcomes is that unphysiological strain induces bone resorption, subsequent to which the Camlog geometry performance deteriorates in comparison to the others. Thus the authors hypothesise that a failure in early osseointegration of the implant surface in the cortical bone affects the optimality of implant geometry. The simulation results of the full bone friction configuration illustrate that a sharp geometrical feature (chamfer in neck) could potentially lead to accelerated bone loss and eventual failure. Limbert et al. [29], in their investigation of trabecular strains and micro-motion (implant displacement) in an embedded Astra implant, reported similar performance implications. There are, however, a few minor distinctions. Limbert et al. used an already osseointegrated implant (and subsequently remodelled adjacent bone) embedded in a porcine mandible segment as the basis for their model. The reported strain magnitudes were largely below unphysiological limits (<3000 με) and were minimally affected by varying the friction coefficients (a higher value corresponds to a firmer bone-implant contact). However, in our study with friction contact, the Camlog implant is observed to induce critical strains at the neck chamfer. These distinctions in the results of the studies can be attributed to the differences in the morphology of human and porcine mandibles, implant geometries tested and boundary conditions. Furthermore, as reported by Wirth et al. in [30,31], bone volume fraction has a direct bearing on the strains transferred through the cortical shell to the trabecular structure. Thus, this study builds upon the established methodology in literature [29–31], by including multiple implant geometries and clinically observed bone morphology, to emphasise the importance of geometry evaluation under closely mimicked clinical conditions.

While distinct implant geometries seem to exhibit differences in performance, it should be noted that from an overall perspective, the failures are not significant in number. The clinical data included in this study consists of a large case pool (3700) with

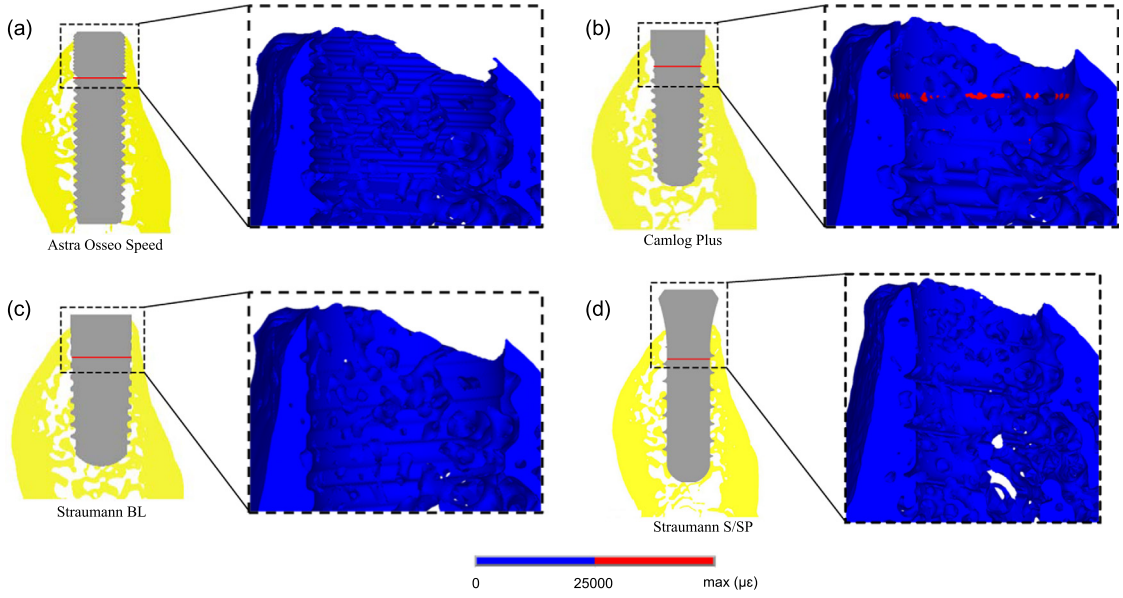

Fig. 7. Strain results (με) for (a) Astra Osseo Speed, (b) Camlog Plus, (c) Straumann BL and (d) Straumann S/SP implants. Above the horizontal red line, relative frictional movement at the bone-implant interface is allowed. Below the red line, the interface is assumed to be fully bonded. The images to the right of each scheme show the distribution, if any, of extremely high strains (>25,000 με) induced in the adjacent bone. For a colour representation, the reader is referred to the online version of this paper. (For interpretation of the references to colour in this figure legend, the reader is referred to the web version of this article.)

low incidence of failures (~0.3%). Additionally there are some modelling and simulation limitations that need to be considered. In terms of the geometry the model were created using a high resolution micro-CT device which limits the object size that can be imaged. Thus the realism of anatomy was limited to a section of the mandible in close proximity to the implant and extrapolated to the rest of the geometry. This makes the whole process of model creation and simulation analysis feasible with modest computational resources. The simulation parameters employed were limited to axial compressive loading in this study. In future studies, the bucco-lingual direction, mesio-distal direction and their combinations would be considered. Furthermore, a more wholesome treatment of this subject must deal with the issue of bone remodelling around the implant. This would involve complex and detailed simulations using an adaptive feedback algorithm based on the mechanostat strain threshold [15,32].

4. Conclusions

In this study the possible correlation between bone loss patterns observed in 10 selected patients and the associated implant geometries was investigated. Using FEA method at the microstructure level, the influence of 4 different implant geometries on the strain patterns in the adjacent bone tissue was analysed. When studied under progressive bone loss patterns observed clinically, the implants showed degraded performance in terms of increased high strain regions in the surrounding bone (>3000 με). The implant geometries were also modelled to simulate an absence of a perfect bond at the bone-implant contact at the upper region of the implant. Results indicate that features such as sharp chamfers can induce localised, extremely high pathological strains (>25,000με).

Thus, while implants geometries are designed to perform under the assumption of osseointegration, when either the bone-implant interface fails or pathological bone loss occurs, the implant geometries might no longer be optimal. This study demonstrates that when evaluating implant geometries, it is imperative to consider not only the best case scenario but also their optimality under progressive bone loss initiated by other factors such as infection and overloading.

Acknowledgements

This work was made feasible due to the cooperation between CEITEC – Central European Institute of Technology (CZ.1.05/1.1.00/02.0068) and regional R&D centre built with financial support from the Operational Programme Research and Development for Innovations within the project NETME Centre (New Technologies for Mechanical Engineering), Reg. No. CZ.1.05/2.1.00/01.0002; and in the follow-up sustainability stage, supported through NETME CENTRE PLUS (LO1202) through grants from the Ministry of Education, Youth and Sports under the National Sustainability Programme I. The sponsoring agencies listed have in no way influenced the outcome of this study. We would like to acknowledge the company MCAE Systems and Miloslav Drápela for their help with the preparation of FE models.

References

[1] Esposito M, Hirsch JM, Lekholm U, Thomsen P. Biological factors contributing to failures of osseointegrated oral implants. (I). Success criteria and epidemiology. Eur J Oral Sci Feb. 1998;106(1):527–51.
[2] Alsaadi G, Quirynen M, Komárek A, van Steenberghe D. Impact of local and systemic factors on the incidence of oral implant failures, up to abutment connection. J Clin Periodontol Jul. 2007;34(7):610–7.
[3] Koldsland OC, Scheie AA, Aass AM. Prevalence of implant loss and the influence of associated factors. J Periodontol Jul. 2009;80(7):1069–75.
[4] Anitua E, Carda C, Andia I. A novel drilling procedure and subsequent bone autograft preparation: a technical note. Int J Oral Max Implan 2007;22(1):138–45.
[5] Wolff J. Das Gesetz der transformation der Knochen, Verlag von August Hirschwald; 1892.
[6] Frost HM. A 2003 update of bone physiology and Wolff's Law for clinicians. Angle Orthod Feb. 2004;74(1):3–15.
[7] Neugebauer J, Scheer M, Mischkowski RA, An S-H, Karapetian VE, Toutenburg H, et al. Comparison of torque measurements and clinical handling of various surgical motors. Int J Oral Max Implan 2009;24(3):469–76.
[8] Shi L, Li H, Fok ASL, Ucer C, Devlin H, Horner K. Shape optimization of dental implants. Int J Oral Max Implan 2007;22(6):911–20.
[9] Achour T, Merdji A, Bachir Bouiadjra B, Serier B, Djebbar N. Stress distribution in dental implant with elastomeric stress barrier. Mater Des 2011;32(1):282–90.
[10] Al-Sukhun J, Kelleway J, Helenius M. Development of a three-dimensional finite element model of a human mandible containing endosseous dental implants. I. Mathematical validation and experimental verification. J Biomed Mater Res Part A Jan. 2007;80(1):234–46.
[11] Field C, Ichim I, Swain MV, Chan E, Darendeliler MA, Li W, et al. Mechanical responses to orthodontic loading: a 3-dimensional finite element multi-tooth model. Am J Orthod Dentofac Orthop 2009;135(2):174–81. Mar..
[12] Ichim I, Kieser JA, Swain MV. Functional significance of strain distribution in the human mandible under masticatory load: numerical predictions. Arch Oral Biol 2007;52(5):465–73.
[13] Marcián P, Konečný O, Borák L, Valášek J, Řehák K, Krpalek D, Florian Z. On the level of computational models in biomechanics depending on gained data from Ct/Mri and micro-Ct. In: MENDEL 2011 – 17th international conference on soft computing; 2011. p. 255–67.
[14] Kayabaşı O, Yüzbasıoğlu E, Erzincanlı F. Static, dynamic and fatigue behaviors of dental implant using finite element method. Adv Eng Softw 2006;37(10):649–58.
[15] Mellal A, Wiskott HWA, Botsis J, Scherrer SS, Belser UC. Stimulating effect of implant loading on surrounding bone. Comparison of three numerical models and validation by in vivo data. Clin Oral Implant Res 2004;15(2):239–48.
[16] Van Oosterwyck H, Duyck J, Vander Sloten J, Van Der Perre G, Naert I. Peri-implant bone tissue strains in cases of dehiscence: a finite element study. Clin Oral Implant Res 2002;13(3):327–33.
[17] Rho JY, Tsui TY, Pharr GM. Elastic properties of human cortical and trabecular lamellar bone measured by nanoindentation. Biomaterials Oct. 1997;18(20):1325–30.
[18] Turner CH, Rho J, Takano Y, Tsui TY, Pharr GM. The elastic properties of trabecular and cortical bone tissues are similar: results from two microscopic measurement techniques. J. Biomech. 1999;32(4):437–41.
[19] Bozkaya D, Muftu S, Muftu A. Evaluation of load transfer characteristics of five different implants in compact bone at different load levels by finite elements analysis. J Prosthet Dent 2004;92(6):523–30.
[20] Chun H-J, Park D-N, Han C-H, Heo S-J, Heo M-S, Koak J-Y. Stress distributions in maxillary bone surrounding overdenture implants with different overdenture attachments. J Oral Rehabil 2005;32(3):193–205.
[21] Gei M, Genna F, Bigoni D. An interface model for the periodontal ligament. J Biomech Eng 2002;124(5):538–46.
[22] Kohles SS, Bowers JR, Vailas AC, Vanderby R. Ultrasonic wave velocity measurement in small polymeric and cortical bone specimens. J Biomech Eng 1997;119(3):232–6.
[23] Menicucci G, Mossolov A, Mozzati M, Lorenzetti M, Preti G. Tooth-implant connection: some biomechanical aspects based on finite element analyses. Clin Oral Implant Res Jun. 2002;13(3):334–41.
[24] Petrie CS, Williams JL. Comparative evaluation of implant designs: influence of diameter, length, and taper on strains in the alveolar crest. A three-dimensional finite-element analysis. Clin Oral Implant Res Aug. 2005;16(4):486–94.
[25] Bujtár P, Sándor GKB, Bojtos A, Szucs A, Barabás J. Finite element analysis of the human mandible at 3 different stages of life. Oral Surg Oral Med Oral Pathol Oral Radiol Endod 2010;110(3):301–9.
[26] Field C, Li Q, Li W, Swain M. Influence of tooth removal on mandibular bone response to mastication. Arch Oral Biol Dec. 2008;53(12):1129–37.
[27] Fujiki K, Aoki K, Marcián P, Borák L, Hudieb M, Ohya K, et al. The influence of mechanical stimulation on osteoclast localization in the mouse maxilla: bone histomorphometry and finite element analysis. Biomech Model Mechanobiol Apr. 2013;12(2):325–33.
[28] Sarrafpour B, Rungsiyakull C, Swain M, Li Q, Zoellner H. Finite element analysis suggests functional bone strain accounts for continuous post-eruptive emergence of teeth. Arch Oral Biol 2012;57(8):1070–8.
[29] Limbert G, van Lierde C, Muraru OL, Walboomers XF, Frank M, Hansson S, et al. Trabecular bone strains around a dental implant and associated micromotions–a micro-CT-based three-dimensional finite element study. J Biomech 2010;43(7):1251–61.
[30] Wirth AJ, Müller R, van Lenthe GH. Computational analyses of small endosseous implants in osteoporotic bone. Eur Cells Mater 2010;20:58–71.
[31] Wirth AJ, Müller R, van Lenthe GH. The discrete nature of trabecular bone microarchitecture affects implant stability. J Biomech 2012;45(6):1060–7.
[32] Lin D, Li Q, Li W, Duckmanton N, Swain M. Mandibular bone remodeling induced by dental implant. J Biomech 2010;43(2):287–93.